

Efficient Parameter Calibration of Numerical Weather Prediction Models via Evolutionary Sequential Transfer Optimization

Heping Fang, Bingdong Li, and Peng Yang, *Senior Member, IEEE*

Abstract—The configuration of physical parameterization schemes in Numerical Weather Prediction (NWP) models plays a critical role in determining the accuracy of the forecast. However, existing parameter calibration methods typically treat each calibration task as an isolated optimization problem. This approach suffers from prohibitive computational costs and necessitates performing iterative searches from scratch for each task, leading to low efficiency in sequential calibration scenarios. To address this issue, we propose the SEquential Evolutionary Transfer Optimization (SEETO) algorithm driven by the representations of the meteorological state. First, to accurately measure the physical similarity between calibration tasks, a meteorological state representation extractor is introduced to map high-dimensional meteorological fields into latent representations. Second, given the similarity in the latent space, a bi-level adaptive knowledge transfer mechanism is designed. At the solution level, superior populations from similar historical tasks are reused to achieve a “warm start” for optimization. At the model level, an ensemble surrogate model based on source task data is constructed to assist the search, employing an adaptive weighting mechanism to dynamically balance the contributions of source domain knowledge and target domain data. Extensive experiments across 10 distinct calibration tasks, which span varying source-target similarities, highlight SEETO’s superior efficiency. Under a strict budget of 20 expensive evaluations, SEETO achieves a 6% average improvement in Hypervolume (HV) over two state-of-the-art baselines. Notably, to match SEETO’s performance at this stage, the comparison algorithms would require an average of 64% and 28% additional evaluations, respectively. This presents a new paradigm for the efficient and accurate automated calibration of NWP model parameters.

Index Terms—Numerical weather prediction, parameter calibration, evolutionary transfer optimization, meteorological state representation, surrogate model.

I. INTRODUCTION

ACCURATE weather forecasting plays an indispensable role in numerous sectors critical to public welfare, including agricultural production [1], aviation and shipping [2],

This work was supported in part by the National Natural Science Foundation of China under Grant 62272210, and Grant 62331014. (Corresponding author: Peng Yang).

Heping Fang is with Department of Statistics and Data Science, Southern University of Science and Technology, Shenzhen 518055, China (e-mail: 12331106@mail.sustech.edu.cn).

Bingdong Li is with the Shanghai Frontiers Science Center of Molecule Intelligent Syntheses, Shanghai Institute of AI for Education, the School of Computer Science and Technology, and the Key Laboratory of Advanced Theory and Application in Statistics and Data Science, Ministry of Education, East China Normal University, Shanghai 200062, China (e-mail: bldli@cs.ecnu.edu.cn).

Peng Yang is with Department of Statistics and Data Science, Southern University of Science and Technology, Shenzhen 518055, China, and also with Guangdong Provincial Key Laboratory of Brain-Inspired Intelligent Computation, Department of Computer Science and Engineering and the Department of Statistics and Data Science, Southern University of Science and Technology, Shenzhen 518055, China (e-mail: yangp@sustech.edu.cn).

energy management [3], and disaster prevention and mitigation [4]. Currently, weather forecasting methodologies are primarily categorized into two mainstream paradigms [5]: Numerical Weather Prediction (NWP) and deep learning approaches. Relying on atmospheric physics and dynamics, numerical simulation methods predict future weather conditions by solving complex systems of Partial Differential Equations (PDEs). Their primary advantage lies in the ability to provide forecast results characterized by strong physical interpretability, spatiotemporal continuity, and high physical consistency [6]. In contrast, deep learning methods, functioning as a data-driven paradigm, excel at learning and identifying complex non-linear patterns from historical meteorological data, demonstrating exceptional computational efficiency during the inference phase. Although deep learning has demonstrated immense potential in certain aspects, numerical simulation remains indispensable for forecasting extreme weather events, maintaining the intrinsic consistency of physical processes, and providing reliable predictions. Therefore, continuously optimizing and enhancing the forecast accuracy of numerical simulation methods remains a crucial task for advancing weather forecasting technology [7], [8].

NWP models are primarily composed of a dynamical core and physical parameterization schemes. These models integrate multiple physical parameterization schemes (e.g., microphysics, planetary boundary layer, and cumulus convection) to meticulously characterize the complex physical processes involved in the evolution of atmospheric states [9]. Note that, the extensive array of parameter values embedded within these schemes significantly influences the accuracy of the final forecast. In practice, researchers typically adopt the default parameter configurations of these schemes. Yet, substantial research indicates that these default settings do not yield optimal forecast results across all geographical regions and weather conditions [10]. Consequently, to enhance forecast precision, error correction of forecast results is required, and calibrating these key parameters for specific weather scenarios has become an essential step in improving NWP performance [5].

The goal of the calibration process is to align the output of complex models with real-world observations. This is achieved by adjusting the model parameters. This has been widely studied in various fields, such as meteorology and finance [11]–[13]. Existing research typically formulates this task as a computationally intensive multi-objective optimization problem. Currently, evolutionary multi-objective optimization algorithms [14]–[18] are the primary approach to solving these problems. However, this approach faces a critical bottleneck. The evaluation of each candidate parameter vector incurs a

high computational cost. Furthermore, a “universal” optimal solution does not exist for the physical parameterization schemes of NWP models. Different calibration tasks are influenced by various factors, such as geographic region and meteorological background. Consequently, researchers must execute independent optimization processes for multiple tasks. These processes are typically performed from scratch and are computationally expensive [8], [19]–[21]. For instance, the calibration of parameters of the Weather Research and Forecasting (WRF) model [13] illustrates this challenge. The WRF is a widely recognized open-source mesoscale NWP model. A single run requires extensive numerical integration of nonlinear atmospheric dynamic equations. This process operates on high-resolution spatiotemporal 3D grids and involves complex physical parameterizations. As a result, it consumes a large amount of computational resources and time [22]. Benchmarks indicate that a single 24-hour simulation at a resolution of 2.5 kilometers consumes approximately 1,150 core hours [23]. Consequently, efficient calibration strategies are essential. Without them, the prohibitive time overhead prevents meeting the requirements for timely forecasting.

In recent years, Surrogate-Assisted Evolutionary Algorithms (SAEAs) [24] have been proposed to address computationally expensive optimization problems. The core philosophy of these methods involves employing computationally inexpensive surrogate models to substitute for the expensive evaluations of the actual physical problems, thereby enabling the efficient search for superior solution vectors using only a limited budget of evaluations. Although existing SAEAs can mitigate the optimization burden for individual parameter calibration tasks of NWP models, the solution process for each task remains isolated when these methods are strictly applied to multiple calibration scenarios, as previously noted. Specifically, each new task initiates its search from a “zero-knowledge” state. This approach, which assumes mutual independence among problems, overlooks a critical reality: real-world problems rarely exist in isolation, and similar tasks often share underlying information that can be exploited. When effectively leveraged, such information can significantly enhance problem-solving efficiency. Recent studies have made methodological advancements in this direction, collectively referred to as Evolutionary Transfer Optimization (ETO) [25]–[27].

Although the application of ETO to multiple calibration tasks of NWP models holds substantial promise for enhancing optimization efficiency, the implementation of this concept encounters three primary challenges [28]. The first challenge is task selection, which aims to identify a subset of source tasks that share similarities with the target task from a comprehensive archive of source tasks. This necessitates a transferability metric tailored to NWP model calibration tasks, capable of accurately quantifying the degree of inter-task similarity. The second challenge is knowledge representation, which involves determining an effective formalism for the information acquired from source calibration tasks, thereby explicitly defining the specific objects to be transferred. The final challenge lies in the knowledge transfer mechanism. Given the discrepancies in objective function landscapes across different NWP calibration tasks, effective adaptive measures

are required to bridge the distribution gap between source and target domains, ensuring that the transferred knowledge can be efficiently utilized during the search process of the target task. To address the aforementioned challenges and facilitate the application of ETO to multiple NWP calibration tasks, we propose the SEquential Evolutionary Transfer Optimization algorithm driven by meteorological state representation, termed SEETO. The main contributions of this study are summarized as follows:

- This study pioneers the application of ETO to address the challenge of repetitive and computationally expensive evaluations inherent in multiple calibration tasks of NWP models. By leveraging knowledge from source tasks related to the target task, the proposed method significantly enhances calibration efficiency.
- We propose a novel approach to guide the parameter calibration of NWP based on the meteorological state itself. A meteorological state representation extraction model based on self-supervised learning is developed. The learned representations are utilized to accurately quantify the similarity between the target task and potential source tasks, thereby enabling the intelligent selection of source tasks for knowledge transfer.
- We design a bi-level adaptive knowledge transfer mechanism. Transfer at the model level is facilitated through the construction of dynamically weighted ensemble surrogate models, while transfer at the solution level is achieved by injecting elite solutions from similar tasks.

The remainder of this paper is organized as follows. Section II provides an overview of the problem background and related work. Section III elaborates on the proposed SEETO algorithm. Section IV presents the detailed experimental design, results, and analysis. Finally, Section V concludes the paper and outlines directions for future research.

II. BACKGROUND AND RELATED WORK

A. Problem Definition

Errors in NWP models predominantly stem from uncertainties associated with physical parameterization schemes. Consequently, a critical question arises regarding how to efficiently determine the optimal configuration of internal parameters within the physical parameterization schemes of NWP models for specific weather forecasting scenarios. We formulate this challenge as the NWP model calibration problem, which is described as follows:

Let $\hat{s} = \{\hat{s}_t\}_{t=1}^T$ denote the observed spatiotemporal variation data of multiple meteorological variables recorded over T time steps. Correspondingly, the NWP model, denoted as $\mathcal{M}(\theta)$, generates predicted spatiotemporal data $s = \{s_t\}_{t=1}^T$ over the same duration. The configuration of parameters θ exerts a direct influence on the generated forecasts. Assuming the existence of an optimal parameter set θ^* such that $\theta^* = \mathcal{M}^{-1}(\hat{s})$, the objective is to determine the value of θ^* . In the literature, this is typically approximated by solving the optimization problem formulated as:

$$\theta^* = \arg \min_{\theta \in \Omega} D(\hat{s}, s = \mathcal{M}(\theta)) \quad (1)$$

where D represents a specific distance metric, typically the Root Mean Squared Error (RMSE) used in parameter calibration. In this study, we select wind speed and temperature in \hat{s} and s as calibration objectives. By adjusting the WRF parameter vector, we aim to simultaneously minimize the forecast errors of these two meteorological variables.

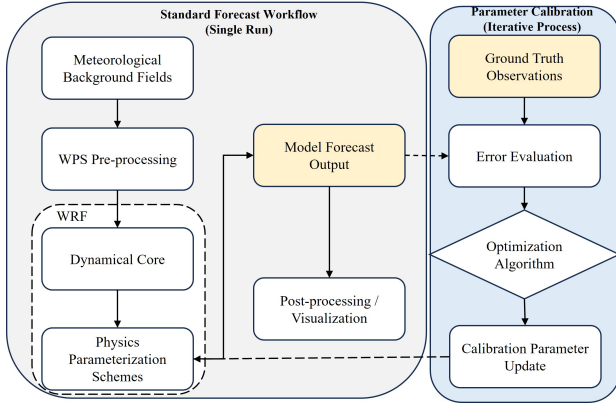


Fig. 1. Flowchart of the NWP Model Parameter Calibration.

B. Calibration of NWP Models

Parameter calibration is a pivotal process for enhancing the prediction accuracy of NWP models. Traditional manual tuning based on empirical experience or “trial-and-error” is not only time-consuming and computationally expensive but also struggles to locate the global optimum within a high-dimensional parameter space. To overcome these limitations, the field has comprehensively shifted towards automatic parameter calibration methods [8], [19]–[21]. The general workflow of such methods is illustrated in Fig. 1, which dynamically adjust parameter configurations based on errors between observational data and forecast results.

Evolutionary Algorithms (EAs) have gained significant traction in this domain due to their robust global search capabilities and proficiency in handling multi-objective optimization problems. However, a single simulation of NPW models typically consumes substantial computational resources and time. To mitigate the bottleneck of exorbitant evaluation costs, SAEAs have been introduced. These approaches utilize computationally inexpensive mathematical models, such as Gaussian Processes (GP) or Neural Networks, to approximate expensive NWP simulations, thereby assisting the algorithm in rapidly converging towards the Pareto optimal front with a limited budget of real evaluations. In recent years, SAEAs have achieved significant success in WRF parameter calibration. For instance, Chinta et al. [20] proposed the Multi-Objective Adaptive Surrogate Model-based Optimization (MOASMO) algorithm, which successfully optimized WRF model parameters and significantly reduced prediction errors for four key meteorological variables during high-intensity rainfall events in the core region of the Indian summer monsoon. Similarly, focusing on the meteorological characteristics of the Beijing area, Wang et al. [19] developed a Knee Point-based Multi-objective Optimization (KMO) algorithm that effectively reduced the number of WRF evaluations via Gaussian Process

surrogates, achieving dual improvements in precipitation and temperature forecast accuracy.

Despite the fact that the aforementioned surrogate-based methods have alleviated computational pressures to a certain extent, they suffer from a fundamental limitation: the lack of a mechanism for reusing historical knowledge. When maximizing performance for each new task, these algorithms are compelled to initialize populations randomly and train surrogate models from scratch. This “amnesic” search paradigm neglects the physical continuity and similarity of meteorological systems across spatiotemporal distributions, forcing the algorithm to expend valuable computational resources on blind exploration during the initial optimization phase, thus making it difficult to achieve an efficient “warm start.”

C. Evolutionary Transfer Optimization

Recent advancements in meta-learning, reinforcement learning, and ETO indicate that the paradigm of problem-solving is shifting towards knowledge reuse, underscoring the potential of leveraging commonalities among similar tasks. While ETO provides a general framework for multi-task problems, tasks in practical applications often arrive dynamically over time, distinguishing them from standard multi-task optimization. Evolutionary Sequential Transfer Optimization (ESTO) [28]–[30] addresses this by utilizing calibration information from historical tasks to accelerate the current task. This form of temporal sequential transfer inherently aligns with the “rolling correction” requirements in meteorological operations. The mathematical formulation of such problems is described as follows:

$$\min_{x \in \Omega} F(x) = \min_{x \in \Omega} (f_1(x | \mathcal{H}), \dots, f_m(x | \mathcal{H})) \quad (2)$$

Here, F denotes the target calibration task, where m determines the number of calibration objectives. x represents the decision vector within the decision space Ω , and \mathcal{H} serves as a knowledge base containing available information from source tasks. Specifically, it is assumed that \mathcal{H} encapsulates the search experience derived from K source tasks, F_1, F_2, \dots, F_K . The ESTO method leverages valid knowledge from \mathcal{H} to accelerate the search process for the target task F . Consequently, a successful ESTO framework is anticipated to achieve faster convergence compared to baseline methods that do not incorporate transfer mechanisms.

Depending on the nature of the transferable knowledge, existing ESTO methodologies can be broadly categorized into three classes: algorithm-based [31], [32], solution-based [30], [33], and model-based approaches [34]–[36]. Among these, solution-based transfer focuses on injecting elite solutions from source tasks directly into the target population, offering high versatility. Conversely, model-based transfer leverages source task data to construct probability distributions or surrogate models, making it particularly well-suited for Expensive Optimization Problems where function evaluations are computationally prohibitive.

In practice, a pool of multiple historical source tasks is often available, giving rise to the Multi-Source Transfer Problem [37], [38]. In this context, the Source Selection mechanism,

which identifies the most promising source tasks from the candidate pool, is critical to the success of the transfer. Existing source selection techniques generally fall into two categories: 1) induction-driven credit assignment [39] and 2) analogy-driven transferability measurement [40]. Induction-driven methods rely on post-transfer feedback to dynamically adjust the weights of source tasks. While flexible during the online phase, the substantial trial-and-error cost incurred at the initial stage is unacceptable for expensive optimization problems. In contrast, analogy-driven methods guide the transfer by pre-calculating task similarity, rendering them more suitable for the "warm start" requirements of expensive optimization. However, existing analogy-driven measurement methods still face two challenges when addressing complex expensive problems such as WRF-based parameter calibration: First, mainstream similarity metrics (e.g., Kullback-Leibler divergence [41], Wasserstein distance [37]) typically require extensive sampling within the decision space to characterize the problem landscape. In expensive optimization scenarios, the extreme scarcity of target task samples makes it difficult for these statistical feature-based methods to accurately estimate distributional discrepancies. Second, existing general-purpose mathematical metrics often overlook the specific physical context of the problem. Relying solely on the distributional distance of solutions in the decision space fails to capture the underlying correlations in physical mechanisms between tasks.

To address these limitations, the NWP parameter calibration task investigated in this study exhibits a unique physical characteristic: similar spatiotemporal distributions of meteorological states often correspond to similar optimal physical parameter configurations. This characteristic provides a novel perspective for designing efficient ESTO frameworks. Utilizing the physical similarity of meteorological states as the criterion for transferability not only circumvents expensive NWP evaluations but also provides more direct and accurate transfer guidance compared to abstract statistical distances.

III. PROPOSED ALGORITHM

A. Framework

Fig. 2 illustrates the overall framework of SEETO. As NWP model calibration tasks arrive sequentially, a SAEA is employed to search for optimal parameter vectors. Throughout this process, data from historical calibration tasks are progressively accumulated to construct a source task data archive (Section III-B). By leveraging this archived data as a knowledge source for the target calibration task, the algorithm can exploit information from similar tasks, thereby circumventing the inefficiency of optimization from scratch. To effectively utilize knowledge from the source task archive, it is essential to identify an appropriate subset of source tasks for transfer. A meteorological state representation extractor (Section III-C) is utilized to extract latent representations for the meteorological states of each task in the archive. Task similarity is then characterized by the distance between the representations of the source and target tasks, which serves as the basis for selecting the optimal source task subset. Subsequently, an adaptive knowledge transfer mechanism (Section III-D)

Algorithm 1 SEETO

Input:

\hat{s}^o : Observed meteorological state series for the target task; $\mathcal{A} = \{(\hat{s}^1, \mathcal{D}^1, G^1), \dots, (\hat{s}^K, \mathcal{D}^K, G^K)\}$: Archive of K source tasks containing states, datasets, and surrogate models; $f(\omega, \cdot)$: Pre-trained meteorological feature extractor; n_p : Population size; FE_{max} : Maximum WRF evaluation budget; γ, Γ : Top- k tasks selection and temperature coefficient for weighting; ρ : Ratio of injected elite solutions; c : Control parameter for dynamic weight β .

Output: PS^* : The optimal Pareto Set for the target task.

```

1: // Task Representation & Similarity Measurement
2:  $z^o \leftarrow f(\omega, \hat{s}^o)$ 
3: for  $i = 1$  to  $K$  do
4:    $sim_i \leftarrow \text{CosineSimilarity}(f(\omega, \hat{s}^i), z^o)$ 
5: end for
6:  $\mathcal{S} \leftarrow \text{SelectTopK}(\mathcal{A}, \{sim_i\}_{i=1}^K, \gamma)$ 
7: Calculate ensemble weights  $\mathbf{w} = \{w_1, \dots, w_\gamma\}$  via Soft-max with  $\Gamma$ :
8:    $w_i \leftarrow \exp(sim_i/\Gamma) / \sum_{j \in \mathcal{S}} \exp(sim_j/\Gamma)$ 
9: // Initialization (Solution-Level Transfer)
10:  $n_{opt} \leftarrow \lfloor \rho \cdot n_p \rfloor$ ;  $\mathcal{P}_{inj} \leftarrow \emptyset$ 
11: for each task  $i \in \mathcal{S}$  do
12:    $n_i \leftarrow \lfloor w_i \cdot n_{opt} \rfloor$ 
13:    $\mathcal{P}_{sub} \leftarrow \text{SelectElites}(\mathcal{D}^i, n_i)$ 
14:    $\mathcal{P}_{inj} \leftarrow \mathcal{P}_{inj} \cup \mathcal{P}_{sub}$ 
15: end for
16:  $\mathcal{P}_{rnd} \leftarrow \text{RandomSampling}(n_p - |\mathcal{P}_{inj}|)$ 
17:  $\mathcal{P} \leftarrow \mathcal{P}_{inj} \cup \mathcal{P}_{rnd}$ 
18: // Evolutionary Optimization (Model-Level Transfer)
19:  $\mathcal{D}^o \leftarrow \phi$ ;  $FE \leftarrow 0$ 
20: while  $FE < FE_{max}$  do
21:    $G_{loc} \leftarrow \text{TrainGP}(\mathcal{D}^o)$ 
22:    $\beta \leftarrow 1 - \exp(-c \cdot FE)$ 
23:   Construct Adaptive Ensemble Surrogate  $G^o$ :
24:    $G^o = (1 - \beta) \sum_{i=1}^\gamma w_i \cdot G_i^s + \beta G_{loc}^{loc}$ 
25:    $\mathcal{P}_{off} \leftarrow \text{EvolvePopulation}(\mathcal{P}, G^o)$ 
26:    $\theta_{new} \leftarrow \text{SelectAcqFunc}(\mathcal{P}_{off})$ 
27:    $\mathbf{F}_{new} \leftarrow \text{EvaluateWRF}(\theta_{new})$ 
28:    $\mathcal{D}^o \leftarrow \mathcal{D}^o \cup \{(\theta_{new}, \mathbf{F}_{new})\}$ 
29:    $FE \leftarrow FE + |\theta_{new}|$ 
30:    $\mathcal{P} \leftarrow \text{UpdatePopulation}(\mathcal{P} \cup \mathcal{P}_{off} \cup (\theta_{new}, \mathbf{F}_{new}))$ 
31: end while
32:  $\mathcal{A} \leftarrow \mathcal{A} \cup (\hat{s}^o, \mathcal{D}^o, G^o)$ 
33: return Non-dominated solutions from  $\mathcal{D}^o$  as  $PS^*$ 

```

facilitates the transfer of knowledge from the selected source task subset to the target task, thereby promoting a "warm start" for the optimization process in the target domain.

The pseudocode of SEETO is presented in Algorithm 1, with detailed descriptions of its constituent sub-modules provided in the subsequent sections.

B. Source Task Archive

In scenarios involving multi-task calibration, traditional methodologies typically discard data generated during the optimization of source tasks, thereby necessitating an independent

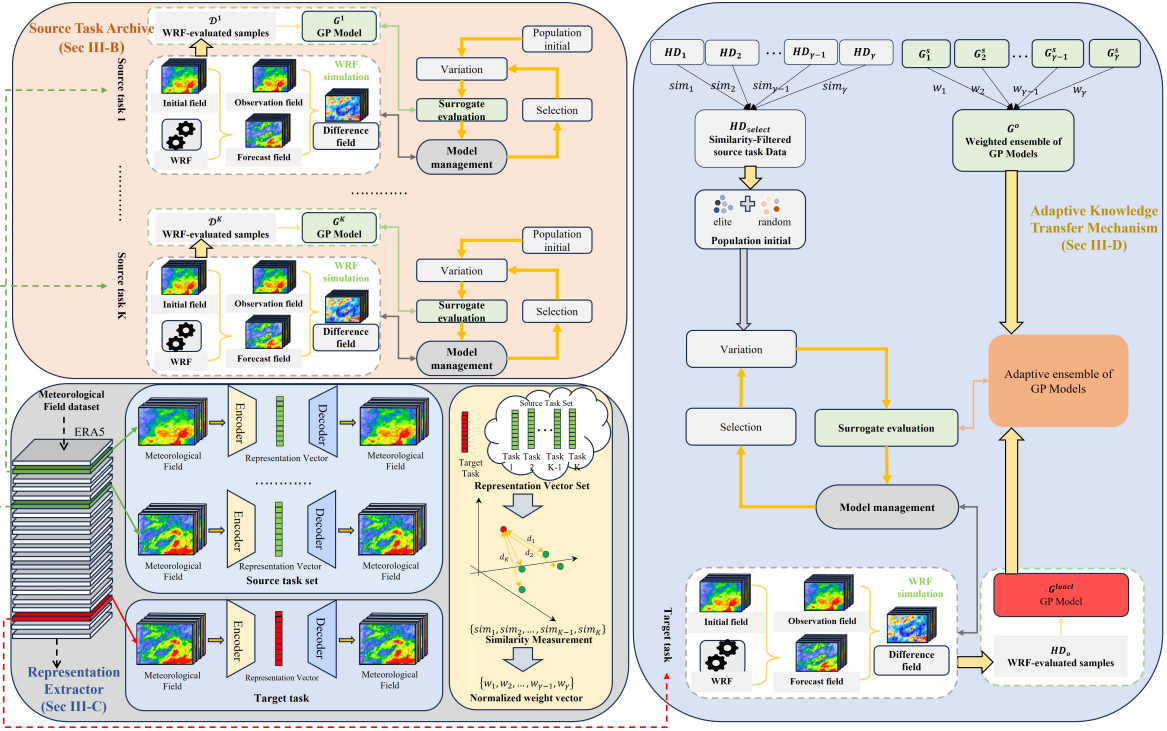


Fig. 2. The framework of the SEETO.

optimization process from scratch for each incoming target task. Consequently, constructing a source task data archive is imperative. As historical calibration tasks accumulate, the repository of transferable knowledge expands, facilitating the rapid adaptation of the optimization algorithm to newly arriving target tasks. The archived data for each source task primarily consists of the following key components:

- **Data Sources for Representation Extraction (\hat{s}^i):** As formulated in Eq. (1), excluding the parameter vector θ to be calibrated, the similarity between a source task and a target task depends on the similarity of their corresponding meteorological states, provided that other NWP model \mathcal{M} configurations remain consistent. Here, a representation extractor is employed to derive a latent representation of the meteorological state for each source task, which serves as the basis for the subsequent calculation of the similarity metric between source and target tasks.
- **Set of Evaluated Solutions (D^i):** During the iterative optimization of each source task, the selected parameter vectors θ are subjected to computationally expensive evaluations via the NWP model \mathcal{M} , and the resulting data are progressively collected. Upon completion of the optimization, the accumulated high-fidelity data pairs (θ, \mathbf{F}) are screened (details provided in Section III-D) to identify the optimal solution set. Injecting this set into a similar target task accelerates the optimization process.
- **Surrogate Model (G^i):** Throughout the optimization of each source task, a GP surrogate model is constructed using the evaluated parameter vectors (θ) and their corresponding forecast performance values (\mathbf{F}) . This model

approximates the mapping between parameter settings and model performance. If a target task exhibits high similarity to a specific source task, the source's surrogate model can be directly leveraged as an auxiliary model. This allows for greater exploration of the optimal solution space under the constraint of limited expensive evaluations.

As the volume of source task data grows, incoming target tasks can evaluate their similarity against a broader array of source tasks, thereby increasing the availability of suitable candidates for effective knowledge transfer.

C. Representation Extractor

In multi-calibration scenarios, effectively leveraging knowledge from existing source calibration tasks to assist a new target task necessitates the identification of physically similar source tasks. Consequently, accurately quantifying the similarity between two tasks emerges as a critical challenge. In the context of parameter calibration, the objective is to minimize the discrepancy between the model output and the known ground truth observed meteorological states. Given that the parameter vector θ serves as the optimization variable while other configurations of the NWP model \mathcal{M} remain consistent, the distinction between tasks is primarily defined by their underlying weather conditions. Therefore, it is sufficient to quantify task similarity by measuring the similarity of the observed meteorological state data characterizing each task.

Let the time series of ground truth observed meteorological state data be denoted as $\{\hat{s}_t\}_{t=1}^T$, where $\hat{s}_t \in \mathbb{R}^{\lambda \times H \times W}$. Specifically, \hat{s}^i and \hat{s}^o denote the meteorological state data for the i -th source task and the target task, respectively. Here,

the meteorological state data consists of λ selected meteorological elements, with each element serving as a distinct channel. The variables W and H denote the width and height of these meteorological elements, respectively. Quantifying the similarity of such meteorological state data constitutes a similarity measurement problem for high-dimensional spatiotemporal data. Traditional metrics typically compute pixel-level errors point-wise; however, they are susceptible to the "Double Penalty" problem [42] and often fail to capture high-dimensional nonlinear spatial features. To address this, we employ a deep learning model for representation extraction, mapping high-dimensional meteorological fields into a low-dimensional latent space. As illustrated in Eq. (3), the task similarity is determined by calculating the average cosine similarity between the corresponding latent representation vectors of the source and target tasks over the time sequence:

$$\begin{aligned} z_t^i &= f(\omega, \hat{s}_t^i) \\ z_t^o &= f(\omega, \hat{s}_t^o) \\ sim^i &= \frac{1}{T} \sum_{t=1}^T \frac{z_t^i \cdot z_t^o}{\|z_t^i\| \|z_t^o\|} \end{aligned} \quad (3)$$

where \hat{s}_t^i and \hat{s}_t^o denote the observed meteorological states for the i -th source task and the target task at time step t , respectively. ω denotes the learnable parameters of the feature extraction network $f(\cdot)$, and z_t^i and z_t^o represent the extracted low-dimensional latent representation vectors.

The representation extraction model comprises two components: an encoder and a decoder. As illustrated in Eq. (4), the encoder consists of multiple downsampling layers and ResNet layers, designed to extract continuous encoded features z_t from the input meteorological state data \hat{s}_t , where the downsampling layers are implemented via 2D convolutions. The architecture of the decoder is the inverse of the encoder, composed of multiple upsampling layers and ResNet layers. Starting from the low-dimensional latent representation vector z_t , it progressively reconstructs the original meteorological state data \hat{s}_t' , with the upsampling layers realized using 2D transposed convolutions. We define the loss function as the reconstruction error between the reconstructed meteorological state \hat{s}_t' and the original input \hat{s}_t . Given that meteorological state data typically consists of continuous physical quantities, the Mean Squared Error (MSE) is adopted as the objective function:

$$\begin{aligned} z_t &= \text{ResNet}(\text{Downsampling}_{\times n}(\hat{s}_t)) \\ \hat{s}_t' &= \text{Upsampling}_{\times n}(\text{ResNet}(z_t)) \\ \mathcal{L} &= \frac{1}{N} \sum_{i=1}^N \left\| \hat{s}_t^{(i)} - \hat{s}_t'^{(i)} \right\|_2^2 \end{aligned} \quad (4)$$

where N represents the number of samples in a training batch, and $\|\cdot\|_2$ denotes the L_2 norm. By minimizing the loss function \mathcal{L} , the model compels the encoder to retain crucial feature information from the original data within the low-dimensional latent vector z_t , thereby achieving high-quality reconstruction.

Based on the cosine similarity between all source tasks and the target task, a set of similar tasks is selected according to a predefined rule. This set contains K source tasks. We

invoke the pre-trained GP surrogate models from this subset. By employing a weighted combination of these models to form an ensemble, knowledge transfer becomes more robust for the target task. This approach provides valuable global guidance during the initial stage of data scarcity, while simultaneously mitigating the risk of being misled by a single erroneous experience through dynamic weight adjustment. On the basis of cosine similarity, the weights for the ensemble model are calculated via normalization as follows:

$$w_i = \frac{\exp(sim_i/\Gamma)}{\sum_{i=1}^K \exp(sim_i/\Gamma)} \quad (5)$$

where Γ is a temperature coefficient. A smaller Γ results in a "sharper" weight distribution; that is, the weights of highly similar tasks approach 1, while those of dissimilar tasks approach 0.

D. Adaptive Knowledge Transfer Mechanism

Building upon the source task subset identified in the previous section, we propose an Adaptive Knowledge Transfer Mechanism. This mechanism reduces the influence of low-similarity source tasks while amplifying the impact of high-similarity ones. Facilitating knowledge transfer at both the model and solution levels, it provides a superior initialization for the optimization of newly arriving target tasks.

- Model Level:** We employ a weighted combination of surrogate models corresponding to multiple source tasks to approximate the current new task. The ensemble model assigns distinct weights to surrogate models from different source tasks, leveraging knowledge captured from different regions of the solution space by models trained in diverse environments. This constructs a more flexible approximation of the complex landscape of the new target task, which shares "partial similarities" with the source task subset. This mechanism serves as a buffer and error-correction strategy, enhancing the robustness of the transfer process. Furthermore, relying solely on an ensemble surrogate model constructed from historical tasks is insufficient to meticulously characterize the unique objective landscape of the new target task as the optimization progresses. Therefore, a local surrogate model is introduced to learn the specific information of the new target task, which is dynamically updated throughout the optimization. Utilizing the ensemble weights derived in Section III-C, we construct an adaptive ensemble surrogate model for the current target task by aggregating the surrogate models G_i^s corresponding to the selected subset of similar source tasks. In this work, GP regression is adopted as the underlying surrogate model. To capture the specific landscape of the target task, a local surrogate model, denoted as G^{loc} , is introduced. As the number of evaluated samples increases, G^{loc} is iteratively updated throughout the optimization process. Consequently, the adaptive ensemble surrogate G^o for the target task is formulated as:

$$G^o = (1 - \beta) \sum_{i=1}^{\gamma} w_i \cdot G_i^s + \beta G^{loc} \quad (6)$$

where $\beta = 1 - \exp(-c \cdot FE)$ represents a dynamic weight, and γ denotes the number of selected source tasks. Here, c regulates the rate of transition from being dominated by the ensemble surrogate model constructed from the source task subset to being dominated by the local surrogate model.

- **Solution Level:** During the optimization process of similar source calibration tasks, solution data evaluated by the NWP model are collected. We reuse the non-dominated solution sets from the collected data, injecting the optimal solution set into the new target task to facilitate a "warm start" of the optimization process. As historical calibration tasks, the optimal solution sets contain valuable information regarding potential regions in the solution space, which is highly beneficial for accelerating the exploration of the optimal solution set for the new target task. In the target task optimization, the population size is set to n_p . The initial population consists of two parts: the injected optimal solution set and a random solution set. The number of optimal solutions is n_{opt} , and the number of random solutions is $n_{ran} = n_p - n_{opt}$. This configuration achieves knowledge transfer while maintaining solution diversity. Utilizing the ensemble model weights obtained in Section III-C, from the expensive evaluation solution set of each task in the similar source task subset, the number of solutions to be extracted is calculated proportional to the weights as $n_i = \lfloor w_i \cdot n_{opt} \rfloor$. To ensure both the convergence and diversity of the injected solutions, we first perform non-dominated sorting on the expensive evaluation solution set of the i -th similar source task, partitioning it into distinct non-dominated levels $\mathcal{F}_1, \mathcal{F}_2, \dots, \mathcal{F}_l$. Based on the relationship between the size of the first non-dominated level $|\mathcal{F}_1|$ and the target extraction count n_i , the final screened optimal solution subset o_i is defined as follows:

$$\begin{cases} \mathcal{T}_{CD}(\mathcal{F}_1, n_i), & \text{if } |\mathcal{F}_1| > n_i \\ \mathcal{F}_1, & \text{if } |\mathcal{F}_1| = n_i \\ (\bigcup_{j=1}^{m-1} \mathcal{F}_j) \cup \mathcal{T}_{CD}(\mathcal{F}_m, n_{other}), & \text{if } |\mathcal{F}_1| < n_i \end{cases} \quad (7)$$

where $\mathcal{T}_{CD}(\mathcal{F}, g)$ represents the crowding distance truncation operator, used to select the top g optimal individuals from set \mathcal{F} based on descending crowding distance. When $|\mathcal{F}_1| < n_i$, the algorithm sequentially absorbs solutions from subsequent levels until the m -th level cannot be fully included. At this point, the remaining number of required solutions is $n_{other} = n_i - \sum_{j=1}^{m-1} |\mathcal{F}_j|$. This strategy ensures that when the number of primary solutions is insufficient, secondary solutions are utilized for supplementation, while prioritizing the retention of non-dominated solutions with the widest distribution when truncating.

IV. EXPERIMENTS

A. Experimental Settings

The experimental evaluation of this study is structured into four primary components:

- A performance comparison of the proposed SEETO against two representative algorithms in the field of WRF parameter calibration, MOASMO [43] and KMO [19], under the constraint of a limited budget of expensive WRF evaluations.
- An ablation study on the adaptive knowledge transfer mechanism, validating its effectiveness by incorporating it into both the MOASMO and KMO algorithms.
- A comparative analysis of the effectiveness of the employed meteorological representation extractor against two related meteorological state extraction algorithms, SCL [44] and AtmoDist [45], within the context of WRF parameter calibration tasks;
- A parameter sensitivity analysis of SEETO to discuss the impact of parameter selection on optimization performance.

To conduct our experiments, the following experimental setup was adopted for the WRF parameter calibration tasks:

- **Calibration Scenario:** The spatial domain for the WRF forecast covers the longitude and latitude range of $38.0^\circ N - 41.75^\circ N$ and $114.5^\circ E - 118.25^\circ E$. The selection of physical parameterization schemes and the parameters to be calibrated for the WRF model is consistent with [19], with details provided in Table I. RMSE is employed as the error metric in the calibration tasks:

$$RMSE = \sqrt{\frac{1}{N \times T} \sum_{i=1}^N \sum_{t=1}^T (s_{i,t} - \hat{s}_{i,t})^2} \quad (8)$$

where $s_{i,t}$ and $\hat{s}_{i,t}$ represent the simulated value and the observed value, respectively, for the i -th grid cell at time step t , and N denotes the total number of grid cells.

- **Data Sources:** Meteorological data were obtained from the ERA5 reanalysis dataset [46] and the China Meteorological Administration Land Data Assimilation System (CLDAS-V2.0) real-time product dataset [47]. ERA5 data serve as the meteorological field input for WRF, providing the necessary data to construct the meteorological states. Since the forecast results output by WRF possess a higher resolution compared to the ERA5 data, the CLDAS dataset is selected as the calibration target (i.e., ground truth observational data) to facilitate calibration at a high precision resolution.
- **Task Sets:** To provide a transferable source task set for SEETO, we partitioned the period from 2017/07/01 00:00 to 2017/07/11 00:00 into $K = 20$ source calibration tasks at 12-hour intervals. The target task set consists of 10 tasks selected from August 2017 (08/03 11:00-08/03 23:00, 08/06 09:00-08/06 21:00, 08/08 14:00-08/09 02:00, 08/12 09:00-08/12 21:00, 08/15 21:00-08/16 09:00, 08/18 15:00-08/19 03:00, 08/21 09:00-08/21 21:00, 08/24 09:00-08/24 21:00, 08/27 20:00-08/28 08:00, 08/29 18:00-08/30 06:00). These are denoted sequentially as "task 1" through "task 10," sorted chronologically, with an interval of approximately 3 days between tasks.
- **Evolutionary Algorithm Configuration:** The population size is set to 100.

TABLE I
PHYSICAL SCHEMES AND PARAMETERS CONFIGURATION.

Physical process	Specific scheme	Parameter	Default	Range	Description
Short-wave radiation	Dudhia shortwave radiation scheme	cssca	0.00001	$[5e^{-6}, 2e^{-5}]$	Scattering tuning parameter(m^2kg^{-1})
Long-wave radiation	RRTM longwave radiation scheme	—	—	—	—
Atmospheric boundary layer	Monin-Obukhov surface layer scheme	—	—	—	—
Land surface	unified Noahland-surface model	porsl	1	[0.5,2]	Multiplier for the saturated soil water content
Cumulus	Kain-Fritsch Eta cumulus scheme	—	—	—	—
Planetary boundary layer	Yonsei University planetary boundary layer scheme	pfac	2	[1,3]	Profile shape exponent used to calculate the momentum diffusivity coefficient
Microphysics	WSM six-class Graupel microphysics scheme	ice_stokes_fac	14900	[8000,30000]	Scaling factor applied to ice fall velocity(s^{-1})
		dimax	0.0005	$[3e^{-4}, 8e^{-4}]$	Limiting maximum value for the cloud-ice diameter(m)

Each problem instance was executed independently 10 times. Since the calibration addresses a computationally expensive multi-objective optimization problem, the optimization performance is measured using Hypervolume (HV), with results presented in the form of mean values and standard deviations.

The hardware and software environment for the experiments is as follows: An AMD Ryzen Threadripper PRO 7985WX processor with 64 cores and 128GB of RAM; the GPU model is an NVIDIA RTX 5880 Ada Generation with 48GB of video memory. The Numerical Weather Prediction model employed is the WRF model version 4.5. The optimization algorithms involved in this study were implemented based on the PlatEMO platform [48].

TABLE II
PARAMETER SETTINGS FOR SEETO

Module	Parameter	Description	Value
Feature Extractor	λ	Number of meteorological state elements	19
Ensemble Surrogate	γ	Number of selected tasks	5
	Γ	Temperature coefficient	0.065
	c	Dynamic weight β control parameter	0.038 or 0.017
	τ	Task similarity threshold	0.7
Solution Injection	ρ	Ratio of injected solutions	0.2
WRF Evaluation	FE_{max}	Max WRF evaluations	60

B. Algorithm Settings

The algorithmic settings required for SEETO are presented in Table II, primarily comprising the following aspects:

- **Meteorological State Representation Extraction:** The meteorological state is composed of multiple meteorological variables, with the selection referencing WeatherBench 2 [49]. This includes 4 single-level variables (2m temperature, 10m u-component of wind, 10m v-component of wind, and mean sea level pressure) and 5 upper-air variables (geopotential, temperature, u-component of wind, v-component of wind, and relative humidity). While the original dataset distributes each

upper-air variable across 13 pressure levels, the number of input variables influences both the accuracy of representation extraction and training costs. To balance accuracy with computational efficiency, the number of meteorological variables is set to $\lambda = 19$ (comprising 5 upper-air variables across 3 distinct pressure levels and 4 single-level variables).

- **Ensemble Surrogate Construction:** The similarity between different target tasks and each source task varies. While high-similarity tasks facilitate transfer, transferring from low-similarity source tasks often leads to "negative transfer." Consequently, the top $\gamma = 5$ similar source tasks from the archive are selected as the source task subset for knowledge transfer. Additionally, the temperature coefficient for similarity normalization is set to $\Gamma = 0.065$, concentrating the ensemble surrogate weights on the most similar source tasks. The control parameter c for the dynamic weight β , which governs the integration of the local surrogate into the ensemble, is set to 0.038 or 0.017. The specific value depends on whether high-similarity tasks exist within the source subset ($w_i \geq \tau$) or not ($w_i < \tau$), where the threshold is set to $\tau = 0.7$.
- **Optimal Solution Set Injection:** In the initial population, the proportion of reused optimal solutions is set to $\rho = 0.2$. Specifically, the initial population consists of $n_{opt} = \lfloor \rho \cdot n_p \rfloor$ optimal individuals reused from past environments, while the remaining $n_{ran} = n_p - n_{opt}$ individuals are randomly generated.
- **Expensive Evaluation in Optimization:** Due to the prohibitive computational cost of Numerical Weather Prediction models, the number of evaluations must be strictly limited. We constrain the maximum number of WRF evaluations to $FE_{max} = 60$.

C. Performance Comparison of Calibration Algorithms

In this subsection, we benchmark the proposed SEETO algorithm against two data-driven evolutionary algorithms, KMO and MOASMO, within the context of WRF calibration tasks. Although these baseline algorithms are designed for solving single calibration problems, this comparative experiment is conducted to validate the effectiveness of SEETO in

TABLE III
COMPARISON OF HV PERFORMANCE AND SEARCH EFFICIENCY

Problem	WRF FE	MOASMO			KMO			SEETO
		HV	$\Delta HV(\%)$	Add.FE(%)	HV	$\Delta HV(\%)$	Add.FE(%)	HV
task 1	20	2.0655E-01 (8.17E-03)	-6.41%	45.00%	2.0655E-01 (8.17E-03)	-6.41%	30.00%	2.1980E-01 (9.17E-04)
task 2	20	1.4097E-01 (6.49E-03)	-6.77%	105.00%	1.4097E-01 (6.49E-03)	-6.77%	35.00%	1.5051E-01 (8.79E-04)
task 3	20	6.1215E-01 (7.90E-03)	-1.46%	30.00%	6.1215E-01 (7.90E-03)	-1.46%	5.00%	6.2110E-01 (7.33E-04)
task 4	20	8.1330E-02 (6.71E-03)	-28.88%	> 200%	8.1330E-02 (6.71E-03)	-28.88%	30.00%	1.0482E-01 (7.05E-04)
task 5	20	5.1515E-01 (6.16E-03)	-1.20%	80.00%	5.1515E-01 (6.16E-03)	-1.20%	25.00%	5.2134E-01 (3.33E-04)
task 6	20	6.0025E-01 (7.21E-03)	-2.11%	25.00%	6.0025E-01 (7.17E-03)	-2.11%	30.00%	6.1289E-01 (6.46E-04)
task 7	20	3.4125E-01 (8.21E-03)	-5.89%	45.00%	3.4125E-01 (8.21E-03)	-5.89%	50.00%	3.6136E-01 (9.95E-04)
task 8	20	5.0341E-01 (7.29E-03)	-1.35%	50.00%	5.0341E-01 (7.29E-03)	-1.35%	50.00%	5.1019E-01 (7.24E-04)
task 9	20	2.7231E-01 (5.41E-03)	-1.25%	25.00%	2.7231E-01 (5.01E-03)	-1.25%	20.00%	2.7572E-01 (8.94E-05)
task 10	20	5.2157E-01 (6.40E-03)	-0.57%	35.00%	5.2157E-01 (6.40E-03)	-0.57%	5.00%	5.2456E-01 (8.02E-04)

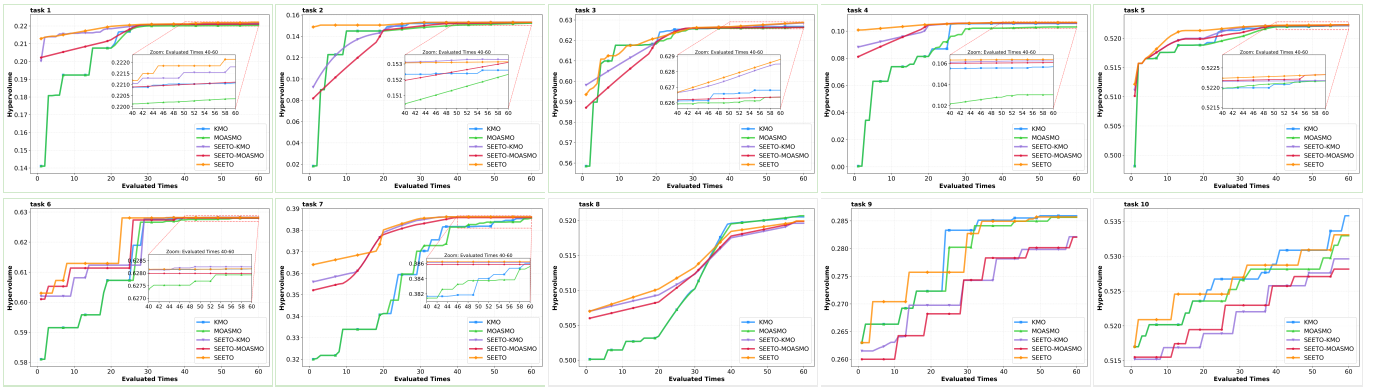


Fig. 3. HV evolution trajectories across 60 WRF evaluations. The subfigures with green background correspond to Tasks 1–7 (Source Tasks), and those with gray background correspond to Tasks 8–10 (Target Tasks).

enhancing performance and mitigating ”cold start” problem following knowledge transfer on the target task set.

Specific settings were adopted for this comparative study. During the initialization phase, both KMO and MOASMO require Quasi-Monte Carlo (QMC) sampling to generate parameter vectors (20 samples, identical for both algorithms), which are subsequently evaluated by WRF to construct the surrogate models for the problem. These methods solve each calibration task independently, without transferring knowledge from the source task archive. Furthermore, by calculating the similarity between the 10 target tasks and the 20 source tasks, we observed that Target Tasks 1-7 could identify highly similar tasks within the source archive, whereas Target Tasks 8-10 could not. This distribution aligns with realistic calibration scenarios.

The comparative results are presented in Table III. Here, $\Delta HV(\%)$ denotes the percentage difference in HV values between the baselines (KMO and MOASMO) and SEETO at the 20-th evaluation; *Add.FE(%)* represents the additional percentage of total evaluation steps required for KMO and MOASMO to achieve the same HV value that SEETO attained at the 20-th step (relative to the base 20 steps). In scenarios characterized by high similarity between the target and source tasks (Tasks 1-7), SEETO demonstrated a distinct computational advantage under the condition of 20 WRF evaluations. Regardless of the varying difficulty across tasks,

SEETO consistently maintained the lead. Taking Task 4 as an example, the performance gap between the baselines and SEETO reached as high as 28.88%. This indicates that within complex parameter calibration landscapes, relying solely on QMC sampling makes it difficult to capture high-quality solutions. In contrast, by integrating historical populations and surrogate models into the optimization process of the current target task, SEETO successfully located superior parameter regions via transferred knowledge. Crucially, the additional computational cost required to bridge these HV gaps is prohibitive. For Task 4, MOASMO required at least an additional 200% of evaluation steps to match the performance level of SEETO at step 20. Even for Task 2, where the gap was smaller, MOASMO still necessitated an expenditure of 105% more computational resources.

Fig. 3 illustrates the evolutionary trajectories of HV for SEETO, KMO, and MOASMO across the complete course of 60 WRF evaluations, clearly delineating the distinct characteristics of each algorithm at different optimization stages. During the initial optimization phase (1–20 evaluations), SEETO demonstrates a significant ”warm start” advantage, particularly in scenarios where the target task shares high similarity with source tasks (Tasks 1–7), SEETO effectively reuses prior knowledge from the source domain, resulting in an initial HV value significantly higher than that of KMO and MOASMO, which begin with a ”cold start.” Conversely, in

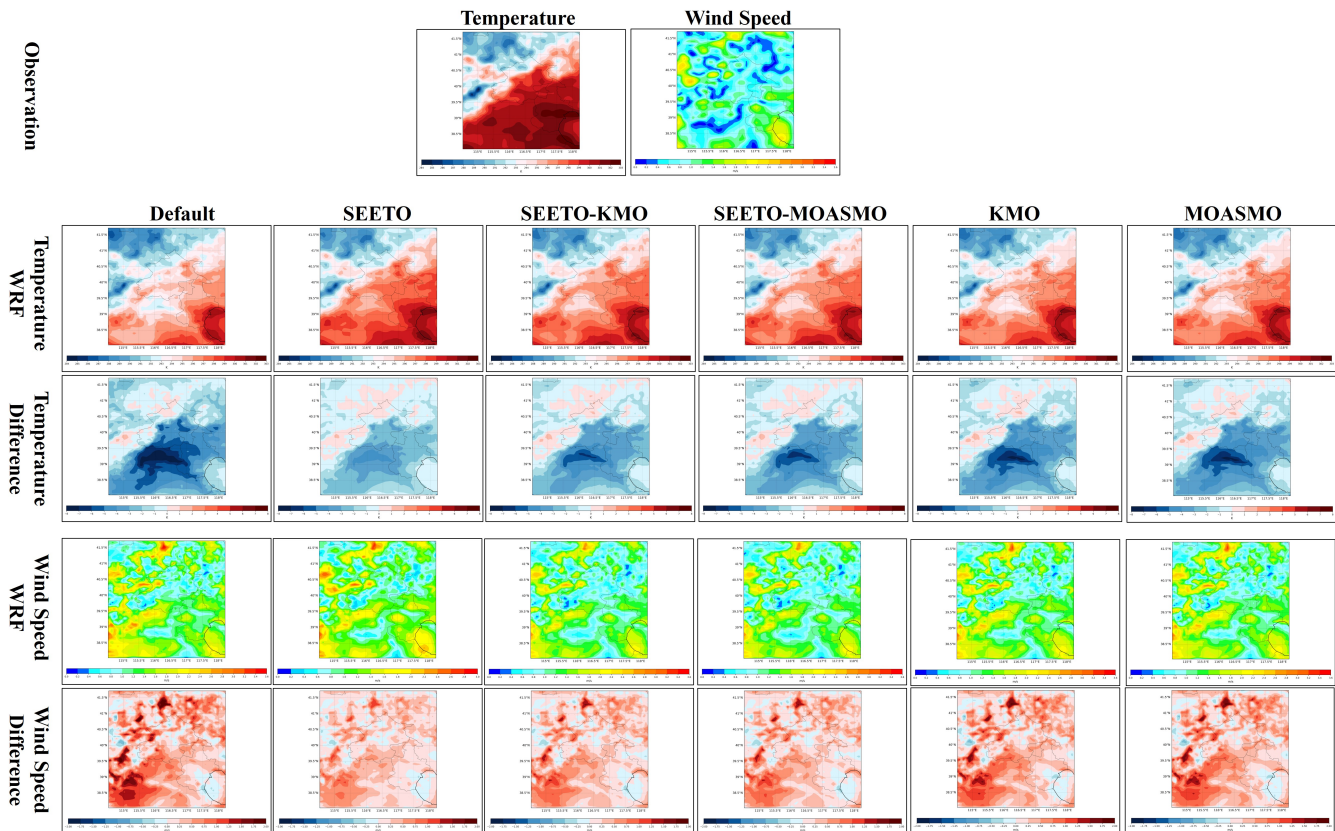


Fig. 4. Visual comparison of forecast fields and error maps for Task 1.

low-similarity scenarios (Tasks 8–10), the initial performance disparity among the three is minimal due to the lack of strongly correlated historical knowledge support. As the number of evaluations progresses to the intermediate stage (21–40 evaluations), the convergence trends of the algorithms exhibit distinct characteristics. Benefiting from the accumulation of sampled data, the surrogate models of KMO and MOASMO gradually fit the current parameter landscape, leading to a rapid improvement in performance. In contrast, the performance growth rate of SEETO decelerates during this phase as it transitions into a fine-grained search stage. In the final optimization phase (41–60 evaluations), performance differentiation across scenarios becomes particularly pronounced. For Tasks 1–7, SEETO maintains its lead throughout the process, demonstrating the robustness of knowledge transfer in related environments. However, it is noteworthy that a “performance inversion” phenomenon emerges in Tasks 8–10, where KMO and MOASMO gradually surpass SEETO in the later stages. This is primarily attributed to the “negative transfer” effect inherent in low-similarity environments—irrelevant prior knowledge from source tasks guides SEETO’s search towards sub-optimal regions, causing its final convergence accuracy to fall short of the comparative algorithms that learn solely from the true feedback of the current task. This finding suggests that while prior knowledge can significantly reduce search costs in high-similarity tasks, the inductive bias introduced in low-similarity contexts may limit the ultimate convergence ceiling of the algorithm over long-term runs.

Fig. 4 provides a visual comparison of the forecast fields generated by the optimal parameter vectors (knee points in the Pareto non-dominated set) found by SEETO, KMO, and MOASMO, alongside the WRF default parameter configuration, for Task 1 after 60 WRF evaluations. It also displays the difference fields between these forecasts and the true observations. First, the comparison of forecast fields in the first row reveals that while the default parameter configuration captures general meteorological trends, it exhibits visible deviations from ground truth in terms of local textures and extremum regions. Post-optimization, the forecast fields generated by SEETO, KMO, and MOASMO are all spatially closer to the true observations. However, the performance disparities among the algorithms are more clearly discerned through the forecast difference maps in the second row. The difference map for the default parameters presents extensive dark regions (representing large positive/negative deviations), indicating significant systematic errors. Although KMO and MOASMO mitigate this bias to a certain extent, as evidenced by the lighter colors in the difference maps, distinct dark error patches persist in specific local regions. This implies that their calibrated parameters failed to completely eliminate local deviations. In contrast, the difference map corresponding to SEETO exhibits the most uniform and faintest hues, indicating the minimal residual magnitude between the forecast and observations. This implies that SEETO not only effectively rectifies the systematic bias of the default parameters but also adjusts physical parameters more precisely than KMO and

MOASMO to fit local micro-meteorological features, thereby achieving the highest forecast accuracy across the entire spatial domain. This visual result corroborates the HV metric analysis presented earlier, confirming that SEETO successfully located parameter combinations with superior physical consistency within a limited computational budget.

D. Ablation on Adaptive Knowledge Transfer Mechanism

To further validate the effectiveness of SEETO’s core component, the Adaptive Knowledge Transfer mechanism, and to assess its generalizability across different benchmark algorithms, we incorporated this mechanism into both KMO and MOASMO algorithms. This resulted in the construction of two derivative variants, denoted as SEETO-KMO and SEETO-MOASMO, which were subsequently benchmarked against their original counterparts. Fig. 3 illustrates the HV evolution trajectories of the algorithms across all 10 tasks, comparing performance before and after the integration of the adaptive knowledge transfer mechanism. Experimental results indicate that the adaptive knowledge transfer mechanism significantly improves the convergence baseline and efficiency of the algorithms in specific scenarios. In scenarios characterized by high similarity between the target and source tasks (Tasks 1–7), SEETO-KMO and SEETO-MOASMO significantly outperform their original versions, KMO and MOASMO. Particularly during the initial optimization phase (1–20 evaluations), the variant algorithms leverage the reuse of historical elite populations to achieve a substantial “warm start” effect. This allows them to rapidly locate regions near the Pareto frontier, whereas the original algorithms remain in an inefficient phase of random exploration. However, in scenarios exhibiting low similarity between the target and source tasks (Tasks 8–10), the inductive bias introduced by the adaptive knowledge transfer mechanism exerts a suppressive effect on algorithmic performance. As depicted in the figure, the final convergence accuracy of SEETO-KMO and SEETO-MOASMO is inferior to that of the original KMO and MOASMO. This phenomenon highlights that when there is a mismatch between the transferred prior knowledge and the current optimization landscape, the forced injection of knowledge biases the search direction, thereby triggering “negative transfer.”

Fig. 4 further provides visual verification of the improvements conferred by the adaptive knowledge transfer mechanism upon the baseline algorithms, specifically from the perspective of spatial error distribution. The variants incorporating the transfer mechanism, SEETO-KMO and SEETO-MOASMO, demonstrate a significant “rectification” capability. Compared to their original versions, the difference fields corresponding to SEETO-KMO and SEETO-MOASMO exhibit noticeably lighter hues, with the previously concentrated dark regions of high error being substantially “smoothed out.” This improvement in the homogeneity of spatial distribution indicates that high-quality prior knowledge from source tasks successfully guided KMO and MOASMO to escape local optima, resulting in generated forecast fields that are physically more consistent with ground truth observations. This visual evidence strongly corroborates the numerical findings, demonstrating that the adaptive knowledge transfer mechanism not

TABLE IV
HV COMPARISON OF DIFFERENT REPRESENTATION LEARNING METHODS

Problem	HV		
	Ours	SCL	AtmoDist
Task 1	2.2214E-01	2.2196E-01	2.1612E-01
Task 2	1.5314E-01	1.5186E-01	1.5095E-01
Task 3	6.2880E-01	6.2713E-01	6.2682E-01
Task 4	1.0639E-01	1.0584E-01	1.0475E-01
Task 5	5.2233E-01	5.2213E-01	5.2083E-01
Task 6	6.2817E-01	6.2732E-01	6.2591E-01
Task 7	3.8624E-01	3.8552E-01	3.8456E-01
Task 8	5.1994E-01	5.1524E-01	5.0133E-01
Task 9	2.8571E-01	2.8442E-01	2.8440E-01
Task 10	5.3309E-01	5.3255E-01	5.2982E-01

only improves the HV metric but also substantively optimizes the accuracy and consistency of forecast results within the physical space.

E. Comparative Analysis of Meteorological State Representation Extraction Methods

To validate the effectiveness of the proposed meteorological state representation extractor in capturing task similarity and guiding transfer optimization, we conducted comparative experiments against two advanced self-supervised representation learning methods in the meteorological domain: SCL and AtmoDist. The final HV obtained in the WRF parameter calibration tasks serves as the primary evaluation metric.

Table IV presents the mean final HV values achieved by the three methods across 10 distinct target tasks. Experimental results indicate that the proposed method achieved superior performance across all tested tasks (Tasks 1–10). Compared to SCL, which is based on spatiotemporal contrastive learning, our method demonstrated a more pronounced advantage in complex tasks. This may be attributed to the fact that SCL primarily focuses on distinguishing categorical features of different weather systems; however, in parameter calibration tasks, capturing subtle spatial structural discrepancies within meteorological fields is of greater criticality. The performance of AtmoDist was relatively weaker. This is likely due to its pre-training objective, which focuses on predicting temporal intervals between atmospheric states. While effective at capturing dynamic evolutionary features, its ability to extract spatial features strongly correlated with physical parameters from static fields at a single time step appears somewhat limited. In contrast, the proposed method reconstructs meteorological states via an encoder-decoder architecture. This forces the latent representations to preserve more comprehensive spatial textures and physical consistency information, thereby providing more precise guidance for the subsequent transfer optimization process.

F. Parameter Sensitivity Analysis

To rigorously evaluate the robustness of SEETO with respect to key hyperparameters and to provide practical guidelines for parameter configuration, this subsection presents a sensitivity analysis focusing on two critical parameters: the

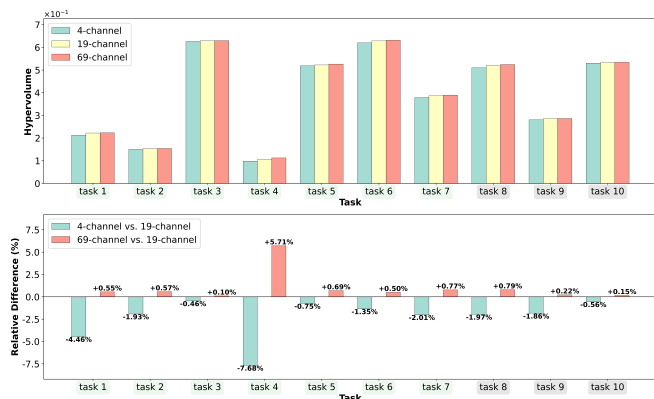


Fig. 5. Parameter sensitivity of λ .

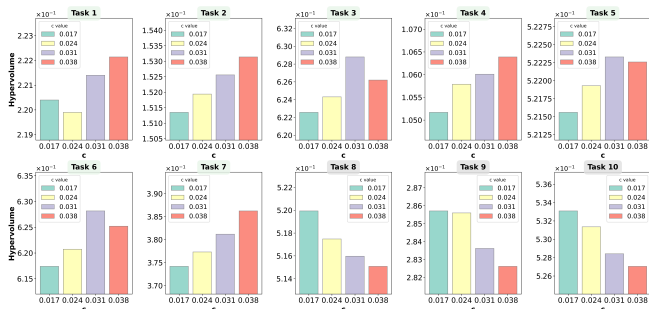


Fig. 6. Parameter sensitivity of c .

number of channels representing the meteorological element dimensions, denoted as λ , and the regulation parameter c , which governs the rate of transition from source domain knowledge to target domain local knowledge.

The richness of the meteorological state representation directly dictates the accuracy of task similarity metrics. We categorized the input channel configurations for the feature extractor into three distinct levels for comparative analysis: a low-dimensional configuration (4 channels, comprising exclusively surface-level variables), a medium-dimensional configuration (19 channels, encompassing surface variables and upper-air variables across 3 key pressure levels), and a high-dimensional configuration (69 channels, including surface variables and the full spectrum of upper-air variables across 13 pressure levels). Fig. 5 illustrates the final HV performance (top panel) and the percentage of relative difference (bottom panel) under these varying channel configurations. Observations from the relative difference plot reveal that, compared to the baseline (19 channels), the 4-channel configuration exhibits a performance degradation across the majority of tasks. Notably, in Task 4, the performance attenuation reaches as high as 7.88%. This suggests that relying solely on surface variables is insufficient to capture complex atmospheric dynamic features, consequently leading to biases in similar task retrieval. In contrast, although the 69-channel configuration yielded positive gains in most tasks, the magnitude of improvement in the remaining tasks was marginal. Considering that incorporating the full set of upper-air variables significantly increases data I/O load and the computational overhead of the feature extraction network,

we conclude that the 19-channel configuration strikes the optimal balance between computational cost and representation effectiveness. Consequently, this configuration is adopted throughout the experiments.

The parameter c governs the rate of transition regarding the dominance of the surrogate model, shifting from the "source task ensemble model" to the "target domain local model" during the optimization process. A larger value of c yields a slower transition rate, predisposing the algorithm to leverage source domain prior knowledge for an extended duration. Conversely, a smaller c value precipitates a more rapid shift towards reliance on the model constructed from local data. Fig. 6 illustrates the trends in HV performance across 10 target tasks with c selected from the set $\{0.0017, 0.0024, 0.0031, 0.0038\}$. Empirical results reveal a significant correlation between this parameter and the source-target task similarity:

Knowledge Exploitation in High-Similarity Scenarios (Tasks 1–7): In these instances, a strong physical correlation exists between the target and source domains. As depicted in Fig. 6, the HV values exhibit an upward trend as the value of c increases. This indicates that in the presence of high-quality prior knowledge, retarding the decay of model weights allows the algorithm to more fully exploit the global guidance capabilities of the source task ensemble model, thereby facilitating accelerated convergence and the discovery of superior solutions.

Negative Transfer Avoidance in Low-Similarity Scenarios (Tasks 8–10): Conversely, for Tasks 8, 9, and 10, the source task archive lacks instances that are highly congruent with the target task. In such cases, larger c values detrimentally impact performance. This suggests that when the reference value of source domain knowledge is limited, a smaller c value accelerates the "forgetting" of irrelevant prior information. This prompts a rapid shift of the search focus towards the surrogate model grounded in local real-time feedback, thereby effectively circumventing the "negative transfer" issue arising from source domain distribution discrepancies. These findings substantiate the pivotal regulatory role of parameter c in handling tasks with varying degrees of correlation.

V. CONCLUSION

To address the challenges of prohibitive computational costs and the inefficiency associated with repetitive optimization from scratch in multi-task NWP model parameter calibration, this paper proposes SEETO. This framework transcends the traditional assumption that calibration tasks are mutually independent. By constructing a knowledge repository of historical tasks, it facilitates a paradigm shift from "isolated trial-and-error" to "knowledge-driven optimization."

In scenarios characterized by high similarity between source and target tasks, SEETO not only exhibits significantly faster convergence speeds compared to benchmark algorithms (KMO and MOASMO) but also achieves optimal levels in terms of both the HV metric of the final solution and spatial forecast accuracy. However, the current method presents certain limitations. In scenarios characterized by low similarity between source and target tasks, although SEETO maintains

a particular initial advantage, "negative transfer" phenomena emerge during the later stages of optimization. This finding indicates that relying solely on static similarity metrics is insufficient to address the dynamically changing search requirements throughout the optimization process. Looking ahead, future work will focus on developing adaptive strategies to dynamically avoid negative transfer, aiming to strike a balance between exploiting historical experience and independent exploration. Concurrently, we plan to extend this framework to high-dimensional multi-objective optimization and heterogeneous transfer scenarios, such as cross-resolution and cross-physics scheme calibration, to accommodate more complex operational meteorological requirements.

REFERENCES

- [1] T. Akilan and K. Baalamurugan, "Automated weather forecasting and field monitoring using gru-cnn model along with iot to support precision agriculture," *Expert systems with applications*, vol. 249, p. 123468, 2024.
- [2] I. Gultepe, R. Sharman, P. D. Williams, B. Zhou, G. Ellrod, P. Minnis, S. Trier, S. Griffin, S. S. Yum, B. Gharabaghi *et al.*, "A review of high impact weather for aviation meteorology," *Pure and applied geophysics*, vol. 176, no. 5, pp. 1869–1921, 2019.
- [3] D. Lazos, A. B. Sproul, and M. Kay, "Optimisation of energy management in commercial buildings with weather forecasting inputs: A review," *Renewable and Sustainable Energy Reviews*, vol. 39, pp. 587–603, 2014.
- [4] G. Camps-Valls, M.-Á. Fernández-Torres, K.-H. Cohrs, A. Höhl, A. Castelletti, A. Pacal, C. Robin, F. Martinuzzi, I. Papoutsis, I. Prapas *et al.*, "Artificial intelligence for modeling and understanding extreme weather and climate events," *Nature Communications*, vol. 16, no. 1, p. 1919, 2025.
- [5] M. Waqas, U. W. Humphries, B. Chueasa, and A. Wangwongchai, "Artificial intelligence and numerical weather prediction models: A technical survey," *Natural Hazards Research*, vol. 5, no. 2, pp. 306–320, 2025.
- [6] M. G. Schultz, C. Betancourt, B. Gong, F. Kleinert, M. Langguth, L. H. Leufen, A. Mozaffari, and S. Stadler, "Can deep learning beat numerical weather prediction?" *Philosophical Transactions of the Royal Society A: Mathematical, Physical and Engineering Sciences*, vol. 379, no. 2194, 2021.
- [7] A. Voudouri, P. Khain, I. Carmona, O. Bellprat, F. Grazzini, E. Avgoustoglou, J. Bettems, and P. Kaufmann, "Objective calibration of numerical weather prediction models," *Atmospheric research*, vol. 190, pp. 128–140, 2017.
- [8] Q. Duan, Z. Di, J. Quan, C. Wang, W. Gong, Y. Gan, A. Ye, C. Miao, S. Miao, X. Liang *et al.*, "Automatic model calibration: A new way to improve numerical weather forecasting," *Bulletin of the American Meteorological Society*, vol. 98, no. 5, pp. 959–970, 2017.
- [9] W. C. Skamarock, J. B. Klemp, J. Dudhia, D. O. Gill, Z. Liu, J. Berner, W. Wang, J. G. Powers, M. G. Duda, D. M. Barker *et al.*, "A description of the advanced research wrf version 4," *NCAR tech. note ncar/tm-556+str*, vol. 145, no. 10.5065, 2019.
- [10] Y. Hiraga and R. Tahara, "Sensitivity of localized heavy rainfall in northern japan to wrf physics parameterization schemes," *Atmospheric Research*, vol. 314, p. 107802, 2025.
- [11] Y. Li, Y. Wu, M. Zhong, S. Liu, and P. Yang, "Simlob: Learning representations of limit order book for financial market simulation," *IEEE Transactions on Artificial Intelligence*, pp. 1–16, 2025.
- [12] C. Wang, J. Ren, and P. Yang, "Alleviating nonidentifiability: a high-fidelity calibration objective for financial market simulation with multivariate time series data," *IEEE Transactions on Computational Social Systems*, 2025.
- [13] P. Yang, J. Ren, F. Wang, and K. Tang, "Towards calibrating financial market simulators with high-frequency data," *Complex System Modeling and Simulation*, 2025.
- [14] W. Hong, G. Li, S. Liu, P. Yang, and K. Tang, "Multi-objective evolutionary optimization for hardware-aware neural network pruning," *Fundamental Research*, vol. 4, no. 4, pp. 941–950, 2024.
- [15] P. Yang, L. Zhang, H. Liu, and G. Li, "Reducing idleness in financial cloud services via multi-objective evolutionary reinforcement learning based load balancer," *Science China Information Sciences*, vol. 67, no. 2, p. 120102, 2024.
- [16] C. Qian, Y. Yu, and Z.-H. Zhou, "Subset selection by pareto optimization," *Advances in neural information processing systems*, vol. 28, 2015.
- [17] B. Li, Z. Di, Y. Yang, H. Qian, P. Yang, H. Hao, K. Tang, and A. Zhou, "It's morphing time: Unleashing the potential of multiple llms via multi-objective optimization," *IEEE Transactions on Evolutionary Computation*, 2025.
- [18] B. Li, Y. Yang, P. Yang, G. Li, K. Tang, and A. Zhou, "Causal inference based large-scale multi-objective optimization," *IEEE Transactions on Evolutionary Computation*, 2025.
- [19] H. Wang, H. Mo, Z. Di, R. Liu, Y. Lang, and Q. Duan, "Knee point-based multiobjective optimization for the numerical weather prediction model in the greater beijing area," *Geophysical Research Letters*, vol. 50, no. 23, p. e2023GL104330, 2023.
- [20] S. Chinta and C. Balaji, "Calibration of wrf model parameters using multiobjective adaptive surrogate model-based optimization to improve the prediction of the indian summer monsoon," *Climate Dynamics*, vol. 55, no. 3, pp. 631–650, 2020.
- [21] H. Baki, S. Chinta, C. Balaji, and B. Srinivasan, "Parameter calibration to improve the prediction of tropical cyclones over the bay of bengal using machine learning-based multiobjective optimization," *Journal of Applied Meteorology and Climatology*, vol. 61, no. 7, pp. 819–837, 2022.
- [22] H. A. Duran-Limon, J. Flores-Contreras, N. Parlavantzas, M. Zhao, and A. Meulenert-Peña, "Efficient execution of the wrf model and other hpc applications in the cloud," *Earth Science Informatics*, vol. 9, no. 3, pp. 365–382, 2016.
- [23] University Corporation for Atmospheric Research. (2022) WRF Version 4.4 Benchmark Data. Accessed: December 26, 2025. [Online]. Available: https://www2.mmm.ucar.edu/wrf/users/benchmark/v44/benchdata_v44.html
- [24] Y. Jin, "Surrogate-assisted evolutionary computation: Recent advances and future challenges," *Swarm and Evolutionary Computation*, vol. 1, no. 2, pp. 61–70, 2011.
- [25] K. C. Tan, L. Feng, and M. Jiang, "Evolutionary transfer optimization—a new frontier in evolutionary computation research," *IEEE Computational Intelligence Magazine*, vol. 16, no. 1, pp. 22–33, 2021.
- [26] W. Lin, Q. Lin, L. Feng, and K. C. Tan, "Ensemble of domain adaptation-based knowledge transfer for evolutionary multitasking," *IEEE Transactions on Evolutionary Computation*, vol. 28, no. 2, pp. 388–402, 2023.
- [27] Z. Cheng, X. Xue, H. Tang, and L. Feng, "Solving expensive dynamic multi-objective problem via cross-problem knowledge transfer," in *International Conference on Neural Information Processing*. Springer, 2024, pp. 264–278.
- [28] X. Xue, C. Yang, L. Feng, K. Zhang, L. Song, and K. C. Tan, "Solution transfer in evolutionary optimization: An empirical study on sequential transfer," *IEEE Transactions on Evolutionary Computation*, vol. 28, no. 6, pp. 1776–1793, 2023.
- [29] X. Xue, C. Yang, Y. Hu, K. Zhang, Y.-M. Cheung, L. Song, and K. C. Tan, "Evolutionary sequential transfer optimization for objective-heterogeneous problems," *IEEE Transactions on Evolutionary Computation*, vol. 26, no. 6, pp. 1424–1438, 2021.
- [30] C. Cao, K. Zhang, X. Xue, K. C. Tan, J. Wang, L. Zhang, P. Liu, and X. Yan, "Global and local search experience-based evolutionary sequential transfer optimization," *IEEE Transactions on Evolutionary Computation*, 2024.
- [31] X. Wu, J. Wu, Y. Zhou, L. Feng, and K. C. Tan, "Towards robustness and explainability of automatic algorithm selection," in *Forty-second International Conference on Machine Learning*, 2025.
- [32] K. Xue, J. Xu, L. Yuan, M. Li, C. Qian, Z. Zhang, and Y. Yu, "Multi-agent dynamic algorithm configuration," *Advances in Neural Information Processing Systems*, vol. 35, pp. 20 147–20 161, 2022.
- [33] L. Zhou, L. Feng, A. Gupta, and Y.-S. Ong, "Learnable evolutionary search across heterogeneous problems via kernelized autoencoding," *IEEE Transactions on Evolutionary Computation*, vol. 25, no. 3, pp. 567–581, 2021.
- [34] Q. Lin, Q. Wang, B. Chen, Y. Ye, L. Ma, and K. C. Tan, "Multiobjective many-tasking evolutionary optimization using diversified gaussian-based knowledge transfer," *IEEE Transactions on Evolutionary Computation*, 2024.
- [35] A. T. W. Min, Y.-S. Ong, A. Gupta, and C.-K. Goh, "Multiproblem surrogates: Transfer evolutionary multiobjective optimization of computationally expensive problems," *IEEE Transactions on Evolutionary Computation*, vol. 23, no. 1, pp. 15–28, 2017.
- [36] M. Shakeri, E. Miah, A. Gupta, and Y.-S. Ong, "Scalable transfer evolutionary optimization: Coping with big task instances," *IEEE transactions on cybernetics*, vol. 53, no. 10, pp. 6160–6172, 2022.

- [37] J. Zhang, W. Zhou, X. Chen, W. Yao, and L. Cao, "Multisource selective transfer framework in multiobjective optimization problems," *IEEE Transactions on Evolutionary Computation*, vol. 24, no. 3, pp. 424–438, 2019.
- [38] Y.-T. Zhong and Y.-J. Gong, "Data-driven evolutionary computation under continuously streaming environments: A drift-aware approach," *IEEE Transactions on Evolutionary Computation*, 2025.
- [39] J. Lin, H.-L. Liu, B. Xue, M. Zhang, and F. Gu, "Multiobjective multitasking optimization based on incremental learning," *IEEE Transactions on Evolutionary Computation*, vol. 24, no. 5, pp. 824–838, 2019.
- [40] Z. Tang, M. Gong, Y. Wu, W. Liu, and Y. Xie, "Regularized evolutionary multitask optimization: Learning to intertask transfer in aligned subspace," *IEEE Transactions on Evolutionary Computation*, vol. 25, no. 2, pp. 262–276, 2020.
- [41] S. Huang, J. Zhong, and W.-J. Yu, "Surrogate-assisted evolutionary framework with adaptive knowledge transfer for multi-task optimization," *IEEE transactions on emerging topics in computing*, vol. 9, no. 4, pp. 1930–1944, 2019.
- [42] C. Subich, S. Z. Husain, L. Separovic, and J. Yang, "Fixing the double penalty in data-driven weather forecasting through a modified spherical harmonic loss function," *arXiv preprint arXiv:2501.19374*, 2025.
- [43] W. Gong, Q. Duan, J. Li, C. Wang, Z. Di, A. Ye, C. Miao, and Y. Dai, "Multiobjective adaptive surrogate modeling-based optimization for parameter estimation of large, complex geophysical models," *Water Resources Research*, vol. 52, no. 3, pp. 1984–2008, 2016.
- [44] L. Wang, Q. Li, and Q. Lv, "Self-supervised classification of weather systems based on spatiotemporal contrastive learning," *Geophysical Research Letters*, vol. 49, no. 15, p. e2022GL099131, 2022.
- [45] S. Hoffmann and C. Lessig, "Atmodist: Self-supervised representation learning for atmospheric dynamics," *Environmental Data Science*, vol. 2, p. e6, 2023.
- [46] H. Hersbach, B. Bell, P. Berrisford, S. Hirahara, A. Horányi, J. Muñoz-Sabater, J. Nicolas, C. Peubey, R. Radu, D. Schepers *et al.*, "The era5 global reanalysis," *Quarterly journal of the royal meteorological society*, vol. 146, no. 730, pp. 1999–2049, 2020.
- [47] National Meteorological Information Center, "CMA Land Data Assimilation System (CLDAS-V2.0)," 2017, accessed: December 26, 2025. [Online]. Available: https://data.cma.cn/data/cdcdetail/dataCode/NAFP_CLDAS2.0_RT.html
- [48] Y. Tian, R. Cheng, X. Zhang, and Y. Jin, "Platemo: A matlab platform for evolutionary multi-objective optimization [educational forum]," *IEEE Computational Intelligence Magazine*, vol. 12, no. 4, pp. 73–87, 2017.
- [49] S. Rasp, S. Hoyer, A. Merose, I. Langmore, P. Battaglia, T. Russell, A. Sanchez-Gonzalez, V. Yang, R. Carver, S. Agrawal *et al.*, "Weatherbench 2: A benchmark for the next generation of data-driven global weather models," *Journal of Advances in Modeling Earth Systems*, vol. 16, no. 6, p. e2023MS004019, 2024.